Resolution Effects in the Hybrid Strong/Weak Coupling Model

by

Zachary R. Hulcher

Submitted to the Department of Physics
in partial fulfillment of the requirements for the degree of

Bachelor of Science in Physics

at the

MASSACHUSETTS INSTITUTE OF TECHNOLOGY

June 2017

Author ..... Signature redacted
Department of Physics
May 12, 2017

Signature redacted
Certified by .....
Krishna Rajagopal
William A. M. Burden Professor of Physics
Thesis Supervisor

Signature redacted
Accepted by .....
Nergis Mavalvala
Marble Professor and Associate Department Head of Physics

Resolution Effects in the Hybrid Strong/Weak Coupling Model

by

Zachary R. Hulcher

Submitted to the Department of Physics
on May 12, 2017, in partial fulfillment of the
requirements for the degree of
Bachelor of Science in Physics

Abstract

Within the context of a hybrid strong/weak coupling model of jet quenching, we study the consequences of the fact that the plasma produced in a heavy ion collision cannot resolve the substructure of a collimated parton shower within it to arbitrary resolution. We introduce a screening length parameter, L_{Res}, proportional to the inverse of the local temperature in the plasma, estimating the value of the proportionality constant from both weakly coupled QCD calculations and holographic calculations appropriate in strongly coupled plasma. We then modify the hybrid model so that when a parton in a jet shower splits, its two offspring are initially treated as unresolved, and are only treated as two separate partons losing energy independently after they are separated by a distance L_{Res}. This modification delays the quenching of partons with intermediate energy, resulting in the survival of more hadrons in the final state with p_T in the several GeV range. We demonstrate that this effect modifies the jet shapes and jet fragmentations functions, as it makes it more probable for particles carrying a small fraction of the jet energy at larger angles from the jet axis to survive their passage through the quark-gluon plasma. We analyze the consequences of different choices for the value of the resolution length L_{Res} on both partonic and hadronic jet shapes and fragmentation functions, as well as on missing-p_T observables. More generally, we discuss the qualitative consequences, and importance, of including the effects of finite resolution.

Thesis Supervisor: Krishna Rajagopal
Title: William A. M. Burden Professor of Physics

Acknowledgments

This thesis would not have been possible without the never-ending guidance and support of both Professor Rajagopal and Dr. Daniel Pablos who welcomed me into their collaboration these last years. I would like to thank Professor Rajagopal for taking me to CERN to work on this project with him and the theorists there, as well as inviting me to present this work in a presentation at the Jets workshop in Paris in Summer 2016 as well as a poster at Quark Matter 2017 in Chicago. I would like to thank Dr. Pablos for all of our meetings in which he guided me through the code and theory as well as cemented my knowledge of the project. I would also like to thank Professor Yen-Jie Lee for introducing me to particle physics and inspiring my love of it. Thank you also to my parents and little brother for supporting my adventures in the field in far away cities and countries.

Contents

Chapter 1

Introduction

Inside the particle detectors at the Relativistic Heavy Ion Collider (RHIC) in Brookhaven, NY and the Large Hadron Collider (LHC) at CERN in Geneva, a super-hot plasma, made of the quarks and gluons normally locked inside protons and neutrons, is created in collisions of heavy ions like lead-lead. This state of matter, Quark-Gluon Plasma (QGP), not seen since the Big Bang when the universe was hot enough to create it, provides a key window into a regime of the strong nuclear force (QCD) not normally immediately accessible in particle accelerators. The strong nuclear force at lower temperatures and energy scales is "strongly coupled," or unable to be analyzed with perturbation theory. This gives it interesting effects uncharacteristic of the conventional gravitational or electromagnetic force like confinement, where the gluons act to keep the strongly colored quarks together in bound states which form the protons and neutrons in an atom as well as other hadrons like pions or kaons. In the hot temperatures created by the collision of the lead ions, the super-relativistic quarks and gluons from the ions interact in a "weakly coupled" way, where perturbation theory applies and the particles behave much more similarly to conventional electrons and photons. The confinement from the strongly coupled regime diminishes such that the quarks and gluons can stream through the superhot medium, which forms a plasma, and behaves like a nearly zero viscosity fluid. Due to this experimentally verified fact, the plasma itself is modeled with the equations of relativistic hydrodynamics. [1, 2, 3, 4, 5, 6, 7]

Because the extremely hot plasma expands and cools very rapidly, dropping the ex-

tremely high temperatures necessary to create and sustain QGP, the plasma is very short-lived. Its lifetime is so short that attempts to identify the plasma and probe it with an external probe are hopeless from the start. Jets, or showers of hadronic matter emanating from a collision, however, offer a probe coming from inside the plasma which can serve this purpose. Jets also occur in collisions where Quark-Gluon Plasma is not created, like in proton-proton collisions, but by comparing with the jets emanating from the heart of the QGP in a lead-lead collision, we gain information about how the jet interacts with the plasma it passes through before hitting the detector. One key effect is that jets lose energy as they pass though the plasma. This process, known as quenching, affects the energy spectrum of the particles in a jet, and also effects the number of particles in the resulting jet, as some may have been able to escape the plasma with enough energy to register on the detector.

As was previously stated, Quark-Gluon Plasma inhabits a temperature region where the strong nuclear force no longer absolutely requires a strongly coupled description, but a weakly coupled, perturbative description can make at least qualitative predictions. Our model combines both of these approaches into the Hybrid Model, which draws from both the weakly coupled and strongly coupled regimes of QCD in order to make predictions for how jets interact with the Quark-Gluon Plasma. With this model in hand, we generate showers of particles using PYTHIA, a Monte Carlo generator for high energy physics, and we insert these showers into a hydrodynamic QGP background. We modify the jet according to the Hybrid Model's predictions of the interactions between the jets and the QGP, and we analyze the resultant showers, comparing various observables to data from the LHC and RHIC.

In this thesis, we begin by briefly reviewing the construction of the Hybrid Model from [8] in Section 2; here, we use the tools of AdS/CFT in order to explore a holographic description of a jet, propagating in the dual of Quark-Gluon Plasma, a Schwarzschild geometry. In Section 3, we then propose a modification to it based on the screening length of strongly charged partons. Particles separated by a small enough distance, characterized by the screening length, which is on the order of the Debye length, should not be resolved from the plasma, as the charges in the plasma shield the particles from all observers, even the

plasma itself, and they should lose energy as one particle in the framework of the Hybrid Model. At a higher level, when color correlated color sources which are sufficiently close to each other propagate through the plasma, then this situation should be physically indistinguishable from the interaction of a particle with the total color charge of the constituents propagating through the same plasma. This physics have been observed in the interference pattern of gluon emissions in a (perturbative) QCD antenna [9, 10, 11], and also in analysis of jet proxies at strong coupling via holography [12].

After discussing the implementation of this resolution effect to the hybrid model in Section 3.1, we will assess its effect on observables from previous works, specifically hadronic jet shapes, fragmentation functions, and two missing pT observables in Section 3.2.

One of our major findings is that when the resolution scale is increased, partons in a jet with lower energy relative to the background cutoff lose less energy over the evolution of the jet while "hiding" in their mother parton. This causes two different effects. First, particles which formerly lost all of their energy, faded into the background, and were removed from the jet now survive to hadronization. Because of this, the fraction of energy carried by the high energy particles decreases while that fraction transfers to the middle energy and specifically the lower energy particles. Another effect observed is that these lower energy particles in the jet are at higher angles relative to the jet center, and so the jet angle widens, and more of the energy is carried at larger angles from the jet center.

Thus, more energy is carried at higher angles in the jet and lower energy particles carry a higher fraction energy relative to those more central in the jet.

We end in Section 4 with a discussion of various results from the calculations, and we point out other avenues for further improvements of our implementation.

Chapter 2

Brief Summary of the Hybrid Model and Previous Modifications

The hybrid strong/weak coupling model is a phenomenological approach to the multi-scale problem one encounters in the jet quenching phenomena description in heavy-ion collisions. The production of high energy jets is under good theoretical control through pQCD calculations due to the high virtuality scale which characterizes the process, and these occur at time scales much shorter than the onset of the QGP. This high virtuality will have to be relaxed by successive splittings, which one should be able to reasonably approximate by the DGLAP (Dokshitzer–Gribov–Lipatov–Altarelli–Parisi) evolution. Indeed, the medium temperature, the relevant energy scale of the QGP, is much smaller than the virtuality carried by these energetic partons and the evolution of the parton shower does not get relevant contributions from the surrounding plasma (this is a good approximation at the earliest stages of the shower, before the partons become nearly on-shell and the virtuality injected by the medium can become important).

Along their passage through the plasma, the partons of the shower will transfer energy and momentum to the medium at a rate that should be described by non-perturbative methods as the typical momentum exchange of such interactions is of the order of the temperature, just nearly above Λ_{QCD}. In order to do so, we model the process by extrapolating results obtained in holography for a certain class of conformal, non-Abelian, strongly coupled gauge theories, where the energy loss of a quark within a plasma is dual to the ab-

sorption of pieces of a string below a black-hole horizon in higher dimensions [13]. This geometric description of energy loss is a new form of intuition with which to gain insight on the challenging strongly coupled dynamics of the jet/plasma interaction. The strongly coupled energy loss rate that we shall use in our model is [8]

$$\left.\frac{dE}{dx}\right|_{\text{strongly coupled}} = -\frac{4}{\pi}E_{\text{in}}\frac{x^2}{x_{\text{stop}}^2}\frac{1}{\sqrt{x_{\text{stop}}^2 - x^2}}, \tag{2.1}$$

where E_{in} is the initial energy of the parton and the stopping distance x_{stop} is

$$x_{\text{stop}} = \frac{1}{2\kappa_{\text{sc}}}\frac{E_{\text{in}}^{1/3}}{T^{4/3}}, \tag{2.2}$$

with κ_{sc} a parameter depending on the 't Hooft coupling constant λ whose precise value depends on the details of the gauge theory at the boundary. For this reason, we use κ_{sc} as a free parameter that shall be fitted to data. We expect it to be smaller in QCD than in $\mathcal{N} = 4$ SYM due to the different number of degrees of freedom at the same energy between the two theories.

In this Section, we provide a brief description of the hybrid model which is the base model whose particle lifetimes we will modify to incorporate the effects of the resolution effect on jets produced in heavy ion collisions that propagate through a droplet of hot matter relative to those produced in proton-proton collisions that propagate in vacuum. A more detailed account of the base model may be found in Refs. [14, 15].

Equation 2.1 gives the rate of energy loss of each particle as it traverses the plasma, and using [14] we take the lifetime of each particle to be

$$\tau = 2\frac{E}{Q^2}, \tag{2.3}$$

where E is the energy of the particle and Q is its virtuality. The factor of 2 connects this equation in the soft limit with the standard expression for formation time.

Equations 2.1 and 2.3 together provide the basis for the hybrid model. Particle split-

tings are generated with PYTHIA using simulated collisions and these particles are given lifetimes according to Equation 2.3. We place the point of origin of the event generated by PYTHIA in the plane transverse to the collision axis at a location proportional to the number of collisions at that point in the transverse plane. We use a Hydrodynamic Profile [14] which initializes at the hydrodynamization time of the plasma, which is τ_{hydro} = .6 fm in this profile. We also take the end of the energy loss to occur at the temperature of the QCD phase transition, such that when the temperature drops below this, the energy loss ceases. The details of this temperature are discussed in [14]. While the particles from the event are in between these two bounds though, the energy loss proceeds according to integration of Equation 2.1, where the temperature experienced by the particle is the temperature of the cell of the Hydro in its local fluid rest frame.

In order to compare this model to data, we still have to fit the one parameter $\kappa_{\rm sc}$, which we do by comparing the model's results for Jet R_{AA}, specifically for jets with transverse momentum, or p_T between 100 and 110 GeV in the range of pseudorapidities from -2 to 2 in the $0-10\%$ most central Pb-Pb events with collision energy $\sqrt{s}$ = 2.76 TeV per collision. After hadronizing the events with PYTHIA's Lund String Model for hadronization and running FastJet's anti-k_T algorithm with various values of R to find the jets from the resultant hadron spectrum, we reproduce jets which can be compared with experiment.[1] By varying $\kappa_{\rm sc}$ in our model to match the CMS data which puts the value of this jet observable between .42 and .51, we find the range of $\kappa_{\rm sc}$ values in accordance with data.

As discussed in previous papers on the Hybrid Model [14, 16, 15], the Hybrid Model has enjoyed excellent success with modeling dijet asymmetry, dijet imbalance, photon-Jet observables, and Z-Jet observables, as these observables are sensitive to the total amount of energy loss, but not to modifications of the shape of the jets.

However, certain effects are missing from this base framework that have been added in previous papers: backreaction and broadening [16], and the hybrid model does not describe as well jet shapes, fragmentation functions, or two of the missing p_T observables.

[1]FastJet groups particles into jets by using a distance measure between particles which is symmetric in the inverse of the particles' transverse momentums (thus, anti k_t) and it also uses R which specifies the angular reach of a jet in the algorithm (also known as the jet radius). The anti k_t groups clusters of particles which are closer in angle than R into a jet and groups particles outside of this range separately. Thus, increasing R and running the algorithm on a previous event set decreases the number of jets found and vice-versa.

Broadening incorporates one physical effect to the Hybrid Model, namely that as the jets propagate through the plasma, they receive kicks transverse to their direction of motion as they propagate through the plasma at a particular angle relative to the jet axis. As one would expect from Brownian motion, this effect, when randomly applied to different particles in the jet acts to broaden and "spread out" the overall jet. If a particle picks up many such kicks, we can approximate the resulting total kick with a Gaussian distribution whose width $Q_\perp^2$ scales with the length, L, the particle propagates, such that $Q_\perp^2 = \hat{q}$ L. By dimensional arguments, $\hat{q} = KT^3$ where K is another fit parameter to be simultaneously fit with $\kappa_{\rm sc}$. This effect does not change the model's production of these observables very noticeably, as these observables are sensitive to the overall jet spectrum of particles as opposed to the total energy loss. The partons in the jet which are most likely to get large transverse kicks are those with small momentum and energy to begin with; these particles are found predominately on the periphery of a jet at large angles relative to the jet axis. These particles suffer much more energy loss due to their decreased energy, and thus the majority of this effect is carried by particles which are energy-lossed out of the spectrum of final particles. Jets get narrower because of the quenching, and these narrow jets, which are broadened much less, do not show the effects of broadening to a large degree.

Backreaction incorporates another physical effect to the Hybrid Model: the energy loss suffered by the partons does not disappear into the proverbial void, but is introduced back into hydrodynamic modes of the plasma itself in order to conserve energy and momentum. This is characterized by the transfer of energy from hard jet modes to soft plasma modes, and a new set of particles is produced in this exchange to carry the energy. We incorporate a linearized relativistic hydrodynamic description of this jet wake according to the Cooper-Frye prescription [16].

This linearized implementation results in a spectrum of particles emitted from the boosted and heated plasma according to

$$\begin{aligned} E\frac{d\Delta N}{d^3p} = & \frac{m_T}{32\pi T^5}\cosh(y-y_j)\exp(\frac{-m_T}{T}\cosh(y-y_j)) \\ & * \{p_\perp \Delta P_\perp \cos(\phi-\phi_j) + \frac{m_T \Delta M_T}{3}\cosh(y-y_j)\}, \end{aligned} \tag{2.4}$$

where p_T, m_T, ϕ, and y are the transverse momentum, transverse mass, azimuthal angle,

and rapidity of the emitted thermal particles transferred to the plasma wake from a jet whose azimuthal angle and rapidity are ϕ_j and y_j.

Broadening and backreaction were added into the Hybrid Model and the observable consequences of this are discussed in [16]. With these two effects, the model still does not fully describe the jet shape and fragmentation function observables. We expect these particular observables to be sensitive to the incorporation of resolution, as resolution will allow the lower energy final particles to survive quenching by propagating as effective emitters, hopefully adjusting the spectrum of particles in the jets to fit these observables more fully.

Thus, with this basis for the Hybrid Model, we move to the discussion of the resolution distance and its incorporation into the Hybrid Model framework.

Chapter 3

Introduction of Resolution Distance into Hybrid Model

Within a deconfined medium of quarks and gluons, a weak coupling analysis of the bremsstrahlung phenomenon consisting of the medium induced radiation of partons off an energetic projectile and its offspring, shows that there is a characteristic length scale, that we shall call $L_{\rm res}$ that depends on the medium properties which sets an upper limit on the resolution power of the plasma. This means that, for instance, a quark-gluon system whose separation is less than $L_{\rm res}$ will be perceived by the plasma as a single colored object with an effective total charge equal to the sum of the two individual charges. However, it is also reasonable to expect that a similar behavior has to occur at strong coupling, where the phenomenon of charge screening is also present as shown by [17]. In order to study the relevance of this effect in jet quenching we estimate next the plasma resolution length $L_{\rm res}$.

Our first important modeling assumption will be to consider that the resolution length is basically dependent on the Debye screening length of the plasma, so that $L_{\rm res} \approx \lambda_D$. The reason is based on the fact that while probe colored charges that sit in different Debye spheres will not be able to affect each other, those sitting within the same Debye sphere will interfere strongly, resulting in a non-independent system of propagating charges as perceived by the plasma. With this choice for $L_{\rm res}$, one concludes that the resolution length is proportional to the inverse local temperature of the plasma in this model. We estimate the proportionality constant with perturbative calculations in the weakly coupled regime

and holographic calculations in the strongly coupled regime.

In the weakly coupled regime, perturbative calculations first presented in [18] calculate the Debye screening length to be approximately $\lambda_D \approx \frac{2.6}{g\pi T}$, where g is the coupling constant. If $\alpha_{QCD} \approx \frac{1}{3}$, then $g \approx 2$, and $L_{\rm res} \approx \lambda_D \approx \frac{1.3}{\pi T}$. On the other side of the spectrum, in the strongly coupled regime, AdS/CFT calculations performed in [17] yield that $L_{\rm res} \approx \lambda_D \approx \frac{0.3}{\pi T}$. This however requires a correction due to the extra degrees of freedom used in AdS/CFT relative to QCD, implying λ_D must be larger by some factor in strongly coupled QCD.

Based on these indications, and for the purpose to perform Monte Carlo calculations within the hybrid model, we keep the scaling of $L_{\rm res}$ with $\frac{1}{\pi T}$, but define a proportionality constant, $R_{\rm res}$ such that

$$L_{\rm res} = \frac{R_{\rm res}}{\pi T}\,, \tag{3.1}$$

so that we can interpolate between these two limiting regimes by changing the value of $R_{\rm res}$. The choice of $R_{\rm res} = 0$ reproduces results without resolution effects. We will explore $R_{\rm res}$ at values of 1 and 2, and in order to check the robustness of our results, the unphysically large limiting case $R_{\rm res} = 5$.

3.1 Implementation of Resolution Effect

In this Section we will present the precise implementation of the finite resolution effect within the hybrid strong/weak coupling model, whose main features have already been described in Section 2.

Until now, the hybrid model has constructed a space-time picture of a parton shower based solely on a formation time argument, such that a specific off-shell parton will split into its two offspring once the formation time for that splitting has passed. This process iterates until all partons are on-shell. By including the effect of finite resolution, we modify not only the space-time picture, but also the total number and the kinematics of the partons in the shower, based on the premise that the medium perceives the propagation of the multi-partonic system as a collection of *effective emitters*: partons whose spatial separation Δx

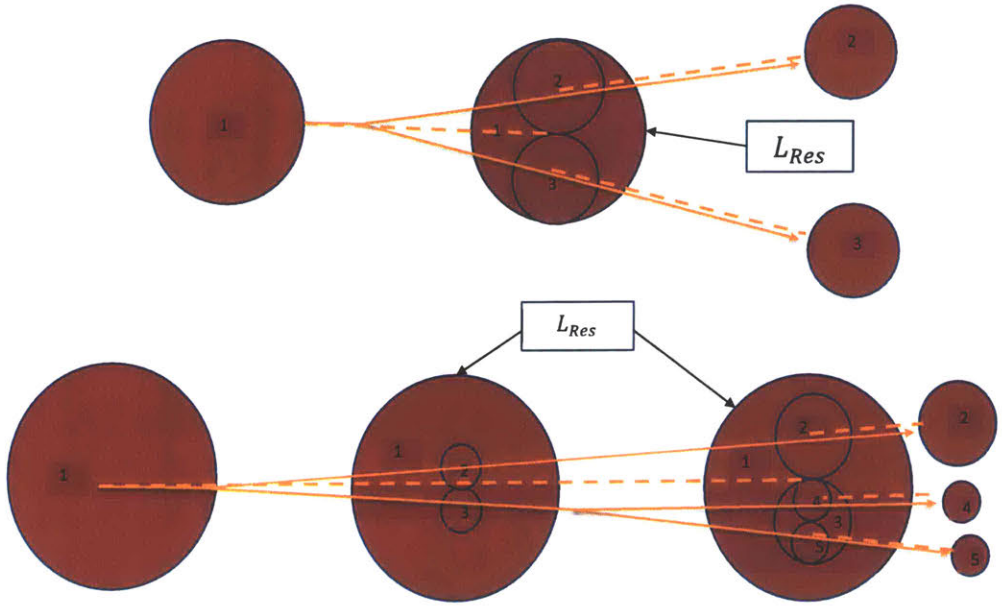

Figure 3-1: A simplified picture of the resolution effect. Solid lines indicate the particle shower without resolution, and dashed lines indicate the new shower with resolution. In the top diagram, particle 1 propagates until its daughters, particles 2 and 3, separate by L_{Res}. In the bottom diagram, the resolution of particles 4 and 5 "breaks" the effective emitter and particle 1 resolves into particles 2, 4, and 5, albeit much later than without resolution.

is less than $L_{\rm res}$ ought to be considered as a single object for the purpose of studying its interaction with the plasma. This fairly simple and straightforward assessment is however not free of implementation ambiguities when applied to a many-body system propagating in a dynamically evolving medium. The precise realization of this mechanism demands a certain degree of modeling and simplifications, required both by consistency and feasibility, that deserve highlighting and shall be discussed next by studying two simple examples.

As the first, most simple example, consider the picture on the top in Fig. 3-1. Here we find depicted a splitting of mother particle m_1 into sister particles s_2 and s_3, which for simplicity are confined in a plane in the diagram. Shown in solid orange lines is the "true" trajectory of the system, determined by the formation time argument only. If one instead requires s_2 and s_3 to be spatially separated more than $L_{\rm res}$ in order to be treated as individual objects from the point of view of the plasma, one would get an "effective" trajectory as shown by the dashed orange lines: the medium perceives that m_1 has lived for a time τ_r, which is longer than the formation time τ_f, and sees particles s_2 and s_3

simultaneously pop up at a different spatial location. Therefore, when we apply our energy loss algorithms on this system, we will need to quench m_1 as if it had propagated until τ_r, and then propagate this energy loss onto its daughters, which after this moment will in turn lose energy as independent sources.

In order to determine τ_r, we need to check at each time step whether the sister spatial separation Δx (a non-local quantity) is greater than $L_{\rm res}$, a quantity that depends on the local temperature of the plasma. Among the different possibilities one could take to determine the value of the temperature and the resultant $L_{\rm res}$, we choose to evaluate it at the space-time point at which the effective emitter sits (the dashed line). Both Δx and $L_{\rm res}$ are compared to each other in the laboratory frame, where the time evolution of the algorithm takes place, in order to avoid issues where we could have s_1 being resolved in the LAB frame at a different time than s_2 due to the lack of absolute simultaneity among different reference frames.

We move now to a more involved, realistic situation, where further splittings can occur before the first two daughters can resolve from each other. This situation is exemplified in the lower picture in Fig. 3-1. Consider m_1 splitting into s_2 and s_3, where s_3 splits into d_4 and d_5 before the spatial separation between s_2 and s_3, this is Δx_{23}, is greater than $L_{\rm res}$. In this example, the first distance to overcome $L_{\rm res}$ is the one between d_4 and d_5, namely Δx_{45}, and not Δx_{23}. Of course, the reader will observe that before $\Delta x_{45} > L_{\rm res}$, s_2 and d_5 will separate by $\Delta x_{25} > L_{\rm res}$, and one could imagine this causing the resolution (assuming for simplicity the same $L_{\rm res}$). The reason why we don't consider such a case is that when d_5 resolves from s_2, d_4 is still unresolved both from s_2 and d_5, meaning that there would be an ambiguity regarding the arrangement of these three partons into effective emitters: should d_4 belong to the effective emitter together with s_2, or to the one with d_5? In order to avoid these and several other ambiguities arising from our phenomenological approach to the problem, we prescribe that the resolution check is to be done in a *closest relative* basis, building effective emitters out from sister particles that can in turn form other effective emitters. In this way, and following the previous example, we never consider the distances Δx_{24} or Δx_{25}, and thus the three particle system behaves as a single emitter, following the trajectory of m_1 until the moment in which $\Delta x_{45} > L_{\rm res}$, where particles s_2, d_4 and d_5

suddenly appear; particle s_3 plays no role in the effective shower and is therefore removed from the effective family tree. Indeed, the resolution between d_4 and d_5 has caused the resolution between s_2 and s_3, since s_3 no longer exists as an effective emitter that could be paired to s_2.

More generally, the logic that we follow to modify the space-time picture of the shower is as follows: first, we fully reconstruct the parton shower by calculating each particle's initial and final position, initial momentum, mother particle, creation time, and splitting (or finishing) time. We step through time incrementally from when a mother splits into its daughters; at each step we recalculate L_{res} from the temperature at the mother's position, and we advance the daughter particles' positions according to their initial velocity, which the energy loss procedure from the hybrid model keeps constant[1]. As a further note, resolutions can only be caused by particles which propagate past τ=.6 due to the discussed start of the hydro profile, and since energy loss does not start until this point either, we enforce that particles which enter the start of the hydro profile are unresolved. We record the first time-step the daughters exceed the resolution distance from their mother, what we shall call the resolution time of the splitting. We add this time for each pair of daughters to the creation time of the daughters and store it in a new variable for each particle, the total resolution time, which will end up being the new creation time for each daughter, as they will not appear and lose energy as their own separate particles until this time. We will modify the lifetimes of the particles in the shower according to this splitting resolution time.

For each event, we enforce on each mother in the event tree that they cannot resolve after any of their daughter particles; if a violation of this is found, we set the resolution time of the mother to that of the daughter, effectively setting the lifetime of the mother to zero. As a second check, we also enforce that sister particles must resolve at the same time, so that if one sister's resolution is forced by one of its children or grandchildren, then the other sister's is as well; if a violation is found, we set the two resolution times equal to the earlier of the two. With continued application of these two checks, when daughter particles resolve, they force the resolution of their mother particle, and their mother particle's mother

[1]This is true only when the broadening mechanism from chapter 2 is absent, as broadening would change the velocities of the particles and introduce changes to the spacings of particles during quenching. Thus, throughout this thesis, we turn broadening off, i.e. we set $K = 0$.

and so on. Thus, sister particles very late in the event which separate very rapidly from each other can drastically change the resolution time of every particle in the sisters' lineage. We continually pass through the particle listing enforcing these two checks until one of the passes does not change anything in the particle listing and we continue.

With this done, we set the new creation time of each particle to be the total resolution time for each particle which was modified from the above loop. Finally, we also advance the initial positions of every particle by the difference between its old creation time and its new creation time multiplied by the recorded initial velocities. The new lifetime of each particle is the difference between the resolution time of its daughter particles and its own resolution time, with final particles getting effectively infinite lifetimes. As a final pass, we delete those particles which have their creation time increased all the way to their finishing time from the particle listing, and we change the mother particle of all the deleted particle's daughters to be the mother of the deleted particle. Our splitting tree has new particle lifetimes, creation times, mothers, and positions, and we quench this new shower in a second run over the particle listing using the new values for the particles' data according to equation 2.1 as described in [16].

Now that we have explained the basic steps and considerations taken to implement finite resolution effects in the hybrid model, which we have found to be the simplest and most unambiguous ones that capture the essential physics, we have attained a solid basis from which to explore the imprint of such mechanism in some crucial jet observables, an analysis to which the next subsection is devoted.

3.2 The Effect of Resolution on Jet Observables

As already outlined in Section 2, the analysis of resolution effects in this work is built on top of the hybrid model without broadening effects, but with medium response. The final result is obtained in terms of hadrons coming both from the hadronization of the parton showers originated in the hard collision as from the perturbed background. Given that our current implementation of medium response is a modification of the background per se, in order to compare to data we need to perform the background subtraction techniques

that experimentalists use for each different observable. The details of these features of the hybrid model can be found in [16].

Before analyzing the effect on some selected jet observables, we want to get an insight on how increasing $L_{\rm res}$ affects the energy loss correlations among the set of final partons (i.e. on-shell partons which are ready to hadronize) within a high energy jet of a given jet radius R. First, for each such final parton we define the quantity $\lambda \equiv E_Q/E_V$, where E_V is the vacuum energy of the parton (or the energy it would have had had there been no medium) and E_Q is the quenched energy due to its propagation through the medium. Now, if all the partons within a jet had lost energy as a single effective emitter, each parton would get the same λ by construction. Therefore, a measure on the size of the effect of finite resolution can be obtained by computing jet-by-jet the distribution for $\lambda/\langle\lambda\rangle$ of each parton within the jet, where $\langle\lambda\rangle$ is the average λ among all those partons. We show in Fig. 3-2 the result for such distribution for different values of $L_{\rm res}\pi T$ (or equivalently $R_{\rm res}$), using partonic anti-kt jets of jet radius $R = 0.3$ with $P_T > 100$ GeV (note that contribution from medium response is not included as it plays no role in the present discussion). Indeed, as expected, the higher $R_{\rm res}$ is, the more this distribution peaks around $\lambda/\langle\lambda\rangle = 1$, getting closer to a δ distribution for the limiting case $R_{\rm res} = 5$.

The reader will observe that the distribution for "No Res" is already fairly peaked around 1, and the reason is two-fold. On one hand, the partons that get completely absorbed by the medium don't make it into the detector and therefore are excluded from this plot; only partons with finite energy can be considered to belong to a jet. On the other hand, the bias imposed by the jet P_T cut, together with the steeply falling spectrum, will tend to favor the presence of narrower, less active jets, that lose on average less energy than more active ones. Narrower jets are originated with a smaller than average virtuality, and therefore the splitting times as computed through the formation time argument will tend to be larger, delaying the presence of independent sources of energy loss within the medium extent. This is also the reason why the distribution is not symmetric around one: the earlier, wider emissions will generally get more quenched than the rest of the system lying around the jet core and, therefore, we will tend to have more partons above the average than below it.

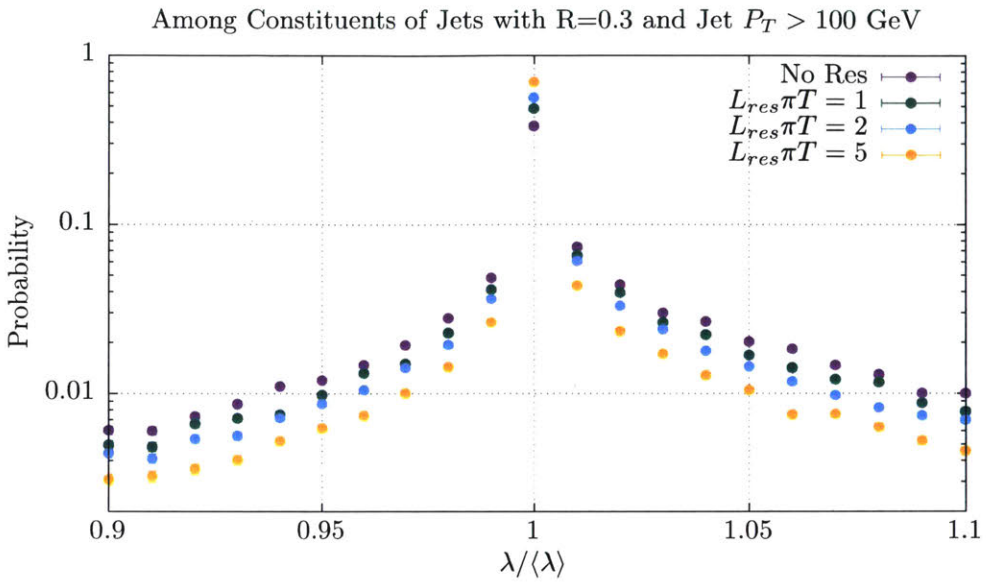

Figure 3-2: An illustration of the quantitative effects of resolution, this histogram plots the λ for a particular particle in a jet normalized by the jet's average λ. As the resolution parameter increases, the jet begins to propagate and lose energy more and more like a single effective emitter, and particles of the jet will approach the 1 bin where all particles lose the same energy. Arbitrarily large angle scatterings in the jet will keep this from ever being a true delta distribution, as those splittings will always be quickly resolved.

Also, please note that the partons considered to be part of a specific jet don't have to come from a single parent parton from the hard scattering, but as in real experiments they can also come from initial state radiation or even from the other (generally back-to-back propagating) hard parton. This yields that even for the limiting case $R_{\text{res}} = 5$ the distribution is not an exact δ function at one.

There are two competing effects when it comes to the recalibration of κ_{sc} due to the inclusion of finite resolution effects. The reduction in the number of effective emitters at a given step of the parton shower evolution within the plasma tends to reduce the amount of total energy loss suffered by the jet, as there are fewer simultaneous sources of energy loss. However, delaying the splitting time of a given parton will allow it to travel more distance within the medium; given the strong path length dependence that the strongly coupled energy loss rate of equation 2.1 has, this can lead to an important increase in the amount of quenching suffered by that parton. While, a priori, the net effect on κ_{sc} is not clear, after performing the full simulations for the different values of R_{res}, and fixing κ_{sc}

in order to reproduce jet R_{AA} for anti-kt jets with jet radius $R = 0.3$ for 0-10% centrality class, for the data point from CMS [19] between $100 - 110$ GeV (as it was done in all our previous papers to constrain the free parameter), we conclude that the values of $\kappa_{\rm sc}$ have to be increased around $10 - 12\,\%$, with small variations between the two finite extreme values of $R_{\rm res}$, namely $R_{\rm res} = 0$, or no Res, and $R_{\rm res} = 5$. This means that the reduction on the number of effective emitters has to be compensated by a reduction of the stopping distances such that jet R_{AA} for those $R = 0.3$ jets stays the same as without the inclusion of resolution effects.

From this fact it makes sense to compute the effect of finite resolution on the cone radius R dependence of jet R_{AA}, given that moderate differences in activity between narrower and wider jets are to some degree reduced when it comes to computing the amount of quenching. In Fig. 3-3 we present results for jet R_{AA} as a function of jet P_T for different values of the cone radius R, for no resolution effects (left panel) and resolution effects with $R_{\rm res} = 2$ (right panel). These results correspond to hadronic jets which have been embedded in the perturbed background and which have gone through the background subtraction procedure described in [16]. As already explained in previous work [16], from the plot in the left of Fig. 3-3 we see how wider jets tend to lose slightly more energy than narrower ones. Even though the overall energy and momentum is conserved within the event, most of the energy flowing from the jet into the hydro modes has been transported at large distances away from the jet axis, which means that for this relatively small jet opening angles one only recovers a small fraction of the total lost energy.

In the right panel of Fig. 3-3, the inclusion of finite resolution effects, as expected, has translated into an even milder dispersion among the jet R_{AA} for the different cone radius R: while the reduction of the stopping distances has brought R_{AA} slightly down for $R = 0.2$, the decrease in the number of effective emitters has made wider jets lose slightly less energy, resulting into a relative confluence of R_{AA} for the different R when compared to the case without resolution effects. This very mild dependence of jet suppression with the cone radius is consistent with published data from CMS [19], although present significantly large error bars prevent us from making a quantitative comparison. Nevertheless, the experimental results are yet another confirmation that lost energy seems to be driven away

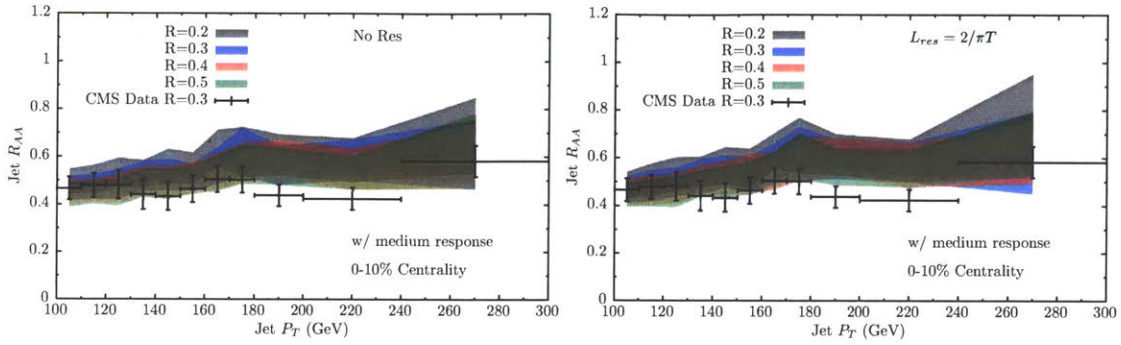

Figure 3-3: These are plots of Jet R_{AA} as a function of P_T for various values of R for both the no Res and R_{res}=2 cases. We see that wider jets tend to lose more energy than narrower jets, and that resolution causes a decrease in the dispersion of R_{AA} with the cone radius, R.

at large angles with great efficiency, giving support to the strongly coupled picture for the jet/plasma interplay in which the energy from the jet hard modes is rapidly converted into hydrodynamic modes over very short lengths. Further precision in this type of measurements will impose great constraints on the details of the energy loss mechanisms at the core of the different jet quenching models in the market, as the different nature of the physics applied will lead to different conclusions regarding the spatial deposition of the lost energy from the jet.

The modification of the spacetime picture of the shower as perceived by the plasma is expected to have implications in the way the jet substructure is affected due to energy loss, as already suggested by the previous observable where there are mild modifications in the treatment of jets with different widths. The softer, relatively wide excitations will see their survival rate increased when compared to the fully resolved case, as they will tend to belong to a composite, more energetic structure with a substantially larger stopping distance. As we said earlier, the need to readjust the jet energy loss through the increase of $\kappa_{\rm sc}$ will therefore reduce those stopping distances, leading to a higher suppression of the harder jet core. We will now see how such jet substructure modifications manifest themselves in two intra-jet observables, namely jet shapes (transverse energy distribution) and jet fragmentation functions (longitudinal energy distribution).

We will start by analyzing the jet shapes, which quantify the fraction of the jet energy in jets reconstructed with anti-k_t parameter R that is contained within an annulus of radius

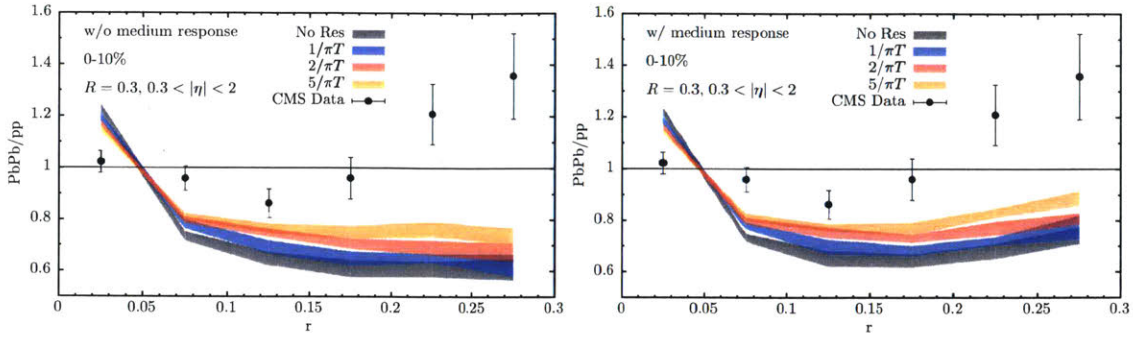

Figure 3-4: Jet shapes characterize the angular distribution of energy relative to the jet axis. We see plotted the effect of resolution without backreaction on the left and with backreaction on the right. Resolution has allowed more particles at wider angles to survive the quenching, resulting in the increase on the right of both figures and the decrease on the left of both figures in the direction of CMS data.

r and width δr (in $\eta - \phi$ space) centered on the jet axis. By following the analysis in Ref. [20], the differential jet shape is defined as

$$\rho(r) \equiv \frac{1}{N_{\text{jets}}} \frac{1}{\delta r} \sum_{\text{jets}} \frac{\sum_{i \in r \pm \delta r/2} p_t^{i,\text{track}}}{p_t^{\text{jet}}} \tag{3.2}$$

for $r < R$, where the particles in the sum don't need to belong to the jet constituents defined through the clustering of the anti-k_t algorithm (normalization to one is imposed in the end). We show in Fig. 3-4 the ratio of jet shapes between quenched jets in PbPb and the ones for vacuum, or pp jets, for the $0 - 10\%$ centrality class. The jets used in this analysis have jet radius $R = 0.3$ and satisfy $p_t^{\text{jet}} > 100$ GeV and $0.3 < |\eta| < 2$. For reference, the experimental results for this ratio are also shown, as measured by the CMS collaboration [20]. The panel in the left shows our results for several values of L_{res} without including the medium response effect, while in the panel in the right such back-reaction effect is taken into account. The previously studied no resolution case is shown in dark grey, and the excessively unresolved case of $R_{\text{res}} = 5$ corresponds to the orange curve. These two limiting cases should be used as references through which to assess the impact of the more physically sensible intermediate values in this observable. As expected, increasing L_{res} increases the probability for wider excitations to make it into the detector and therefore the selection bias towards narrower jets is less pronounced than without resolution effects. This

effect amounts to a depletion of the energy fraction lying at the very core of the quenched jet in favor of contributions at a wider annulus, which translates into a more homogeneous modification of the angular substructure, as seems to be suggested by data. Of course, the fact that we are comparing medium and vacuum jets at the same final energies implies that the quenched distribution ends up having a higher relative contribution from narrower jets, as it is known that the jet shapes become narrower with increasing transverse momentum.

Despite the relative success in the description of the angular structure of the central region, the notable enhancement of the jet shape in PbPb with respect to vacuum at the periphery of the jet is clearly misrepresented by the left panel, due to the absence of the energy contribution coming from the wake. Indeed, by including the soft and wide angle hadrons coming from the decay of the wake at the freeze-out hypersurface induced by the jet passage, we see in the panel in the right that these small energy depositions have important consequences at the tail of the jet shape, where the relative energy contribution is around a mere 2% of the total. Nevertheless, interesting quantitative differences with respect to data remain, which most likely point to the need of having a simulation of the medium response which goes beyond the small perturbations approximation described in [16]. In this way, while the finite resolution effect appears to be important in the understanding of the angular structure of energy within the jet, it is clearly not enough to account for the phenomenon across all angularities without the inclusion of a more realistic treatment of hydro response to the jet passage.

The next intra-jet observable, the jet fragmentation function, corresponds to a characterization of the longitudinal energy fraction that charged hadrons within a jet carry with respect to the total energy of the jet. The tracks used in the analysis lie within a distance r from the jet axis in the $\eta - \phi$ plane, and the distribution is expressed in terms of the variable $\ln(1/\mathrm{z})$, with z defined as $z \equiv p_{\mathrm{track}} \cos\theta / p_{\mathrm{jet}}$, where θ is the angle between the jet axis and the momentum of the track. As in the previous observable, we show in Fig. 3-5 two panels for the ratio of the quenched fragmentation functions over the vacuum ones, with medium response (right panel) and without it (left panel). The contribution from the hardest tracks lying around $z \sim 1$ is diminished by increasing L_{res}, while the one for the relatively soft particles around $\ln(1/\mathrm{z}) \sim 3$ is enhanced. Analogously to what we discussed regarding

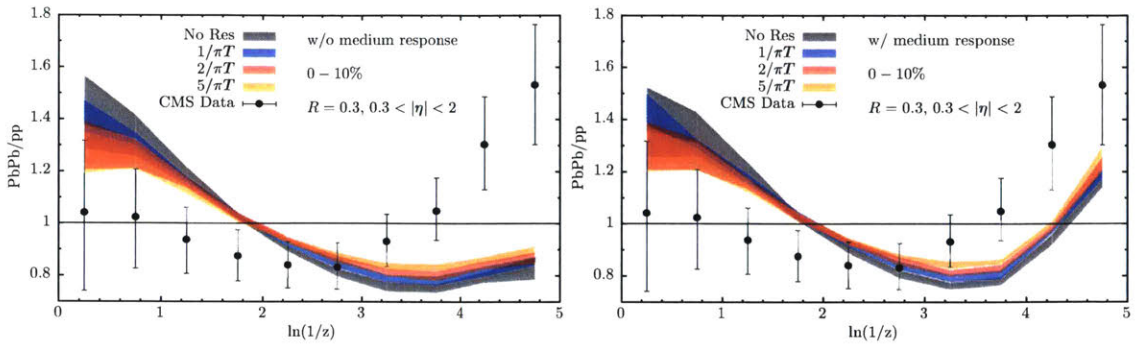

Figure 3-5: Fragmentation functions characterize longitudinal energy fraction carried by particles relative to the total energy of the jet. We see plotted the effect of resolution without backreaction on the left and with backreaction on the right. Resolution has allowed more of the particles with lower energy fractions to survive the quenching, resulting in the increase on the right of both figures and the decrease on the left of both figures, in the direction of CMS data.

the enhancement of the relative peripheral energy for the jet shapes ratio, the rise seen in data at smallest z of the PbPb fragmentation functions with respect to the pp ones cannot be explained only through finite resolution effects and requires the contribution of the medium response. Although those particles belonging to the wake are indeed a necessary ingredient to describe the internal soft structure of a quenched jet, the inclusion of the finite resolution distance $L_{\rm res}$ allows us to understand the mild modifications of the harder and central parts of the intra-jet distributions seen in experiments as being due to a relatively coarse-grained quenching of an unresolved perturbative shower.

We can further explore the consequences of the existence of a minimum resolution length by analyzing the so called "missing-pt" observables, which allow for a complete characterization of the momentum and angular correlations of all the particles in a dijet event with respect to the axis defined by such dijet. While this is an excellent observable with which to study the jet/plasma interplay details by the presence of the medium response mechanism, [16], here we want to focus on the potential modifications that finite resolution induces due to the different internal structure between the leading and the subleading jet of the dijet pair.

More specifically, this set of observables are distributions of the quantity $\not{p}_{\rm T}^{\parallel}$, calculated

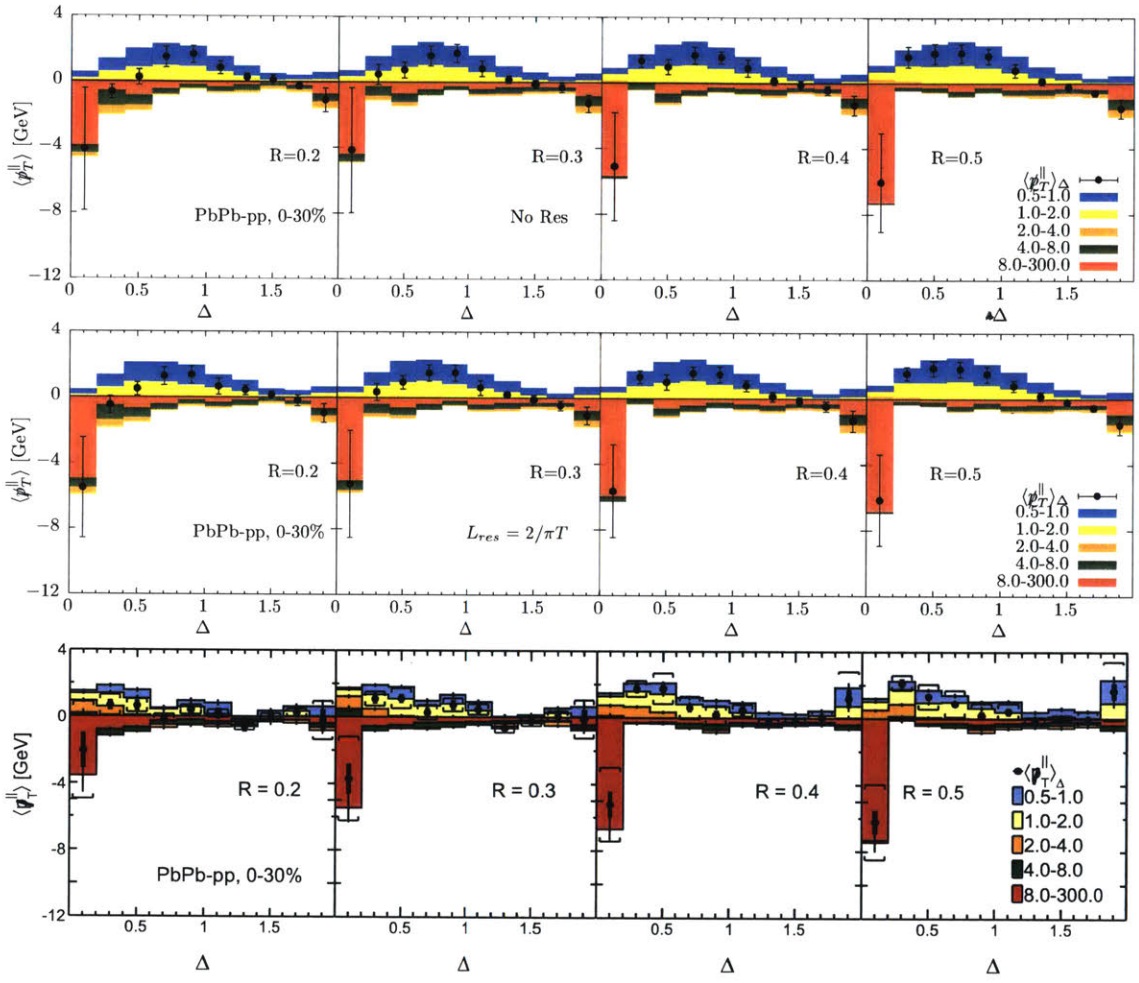

Figure 3-6: This missing P_T observable characterizes the asymmetry between the spectrum of the leading and subleading jets according to Equation 3.3. The effect of resolution can be seen to be a slight improvement relative to data, but the "orange problem" of previous works is still present, albeit reduced.

for every track in the event, and defined as

$$\not{p}_{\mathrm{T}}^{\parallel} \equiv -p_{\mathrm{T}} \cos\left(\phi_{\mathrm{dijet}} - \phi\right) , \tag{3.3}$$

where p_{T} and ϕ are the transverse momentum and the angle of the track respectively, and ϕ_{dijet} is the bisection angle between the leading jet angle ϕ_{leading} and the flipped subleading jet angle $-\phi_{\mathrm{subleading}}$. With such definition, tracks in the subleading jet hemisphere give positive contributions to $\not{p}_{\mathrm{T}}^{\parallel}$, while those in the leading jet hemisphere contribute negatively. We only consider dijet pairs with leading and subleading transverse momenta ${p_{\mathrm{T}}}^{\mathrm{leading}} > 120$ GeV and ${p_{\mathrm{T}}}^{\mathrm{subleading}} > 50$ GeV respectively, with both jets lying within $|\eta| < 2$. We also enforce a back-to-back criterion of $\Delta\phi > 5\pi/6$ between the two jets. In order to cover as much angular separation as possible, and once the dijet has been properly identified, we restrict their pseudorapidity range to be within $|\eta| < 0.6$. These are the same experimental cuts used in Ref. [21].

In the first two panels of Fig. 3-6 we show our results for the difference $\not{p}_{\mathrm{T}}^{\parallel}$ distribution between PbPb and pp, as a function of Δ (the angular separation of the tracks in $\eta - \phi$ plane with respect to either the leading or the subleading jet axis, depending on which yields a smaller Δ) for dijet events reconstructed with different anti-k_t radius R, together with a third panel with the results published by the CMS collaboration [21]. The contributions to $\not{p}_{\mathrm{T}}^{\parallel}$ are further sliced into different p_{T} bins, represented by the different colors, and whose total sum is shown by the black dots. The top panel shows results without any resolution effects, and the mid panel is obtained by setting $R_{\mathrm{res}} = 2$. As argued before, this specific choice serves to illustrate the typical size of the effect on observables induced by the mechanism under consideration. Differences between the top two panels are small, but visible. By including finite resolution, one can see how for the smallest Δ bin the green contribution to $\not{p}_{\mathrm{T}}^{\parallel}$, corresponding to tracks with $4 \leq p_{\mathrm{T}} < 8$ GeV, changes sign going from an excess in the leading jet side to an excess in the subleading jet side, which is in good agreement with what is seen in data. Also consistent with the data, for the rest of the Δ bins a noticeable reduction of the excess of the green contribution on the leading jet side is observed. Indeed, this is an indication that particles well below the total energy of the jet,

thus belonging to relatively active jets, are more likely to survive than without resolution effects, making it easier for such kind of jets to pass the cuts and enter the distribution. (Recall that, by construction, the subleading jet is the one with lower energy of the pair and therefore has had to lose more energy on average than the leading jet. This is why in the subleading jet side we encounter at relatively large angles all the softer particles coming from the wake that fulfill global energy-momentum conservation event by event). The same observation can be applied to the orange bin, corresponding to $2 \leq p_{\mathrm{T}} < 4$ GeV particles, although despite the improvement, for this momentum regime the discrepancy with data is still significant, especially for the lowest Δ bins: this is what we called the "orange problem" in our previous work. Even though the jet samples are different, the tension arising in this observable is very likely to be correlated with the current failure of our model to describe quantitatively the enhancement at the tail of the jet shapes ratio for small jets with an anti-k_t radius of $R = 0.3$, a failure that we think indicates the need for a more complete treatment of backreaction which would generate different hadronic spectra from the jet wakes in the plasma.

A different way to present the physics contained in Fig. 3-6 consists in presenting such $\not{p}_{\mathrm{T}}^{\parallel}$ distributions integrated in Δ, and sliced instead in terms of the dijet asymmetry variable $A_J \equiv (p_{\mathrm{T}}{}^{\mathrm{leading}} + p_{\mathrm{T}}{}^{\mathrm{subleading}})/(p_{\mathrm{T}}{}^{\mathrm{leading}} - p_{\mathrm{T}}{}^{\mathrm{subleading}})$. This is done in Fig. 3-7, for two different centrality classes, with the top two panels corresponding to our simulations and the bottom panel showing CMS data [21]. In these plots, only dijets made from jets with anti-k_t radius $R = 0.3$ are considered. While the two hardest p_{T} bins, the red and green, appear to be well described by our model when compared to data once we include the finite resolution effects in the mid panel of Fig. 3-7, there is a clear cancellation in data between the orange contribution from the leading and the subleading jet hemispheres that is not correctly captured by our simulations, especially for the most central collisions. Presumably, this too can be attributed to the oversimplified procedure we have conducted to compute the hadronic spectra coming from the wake generated in the plasma due to the passage of the jet.

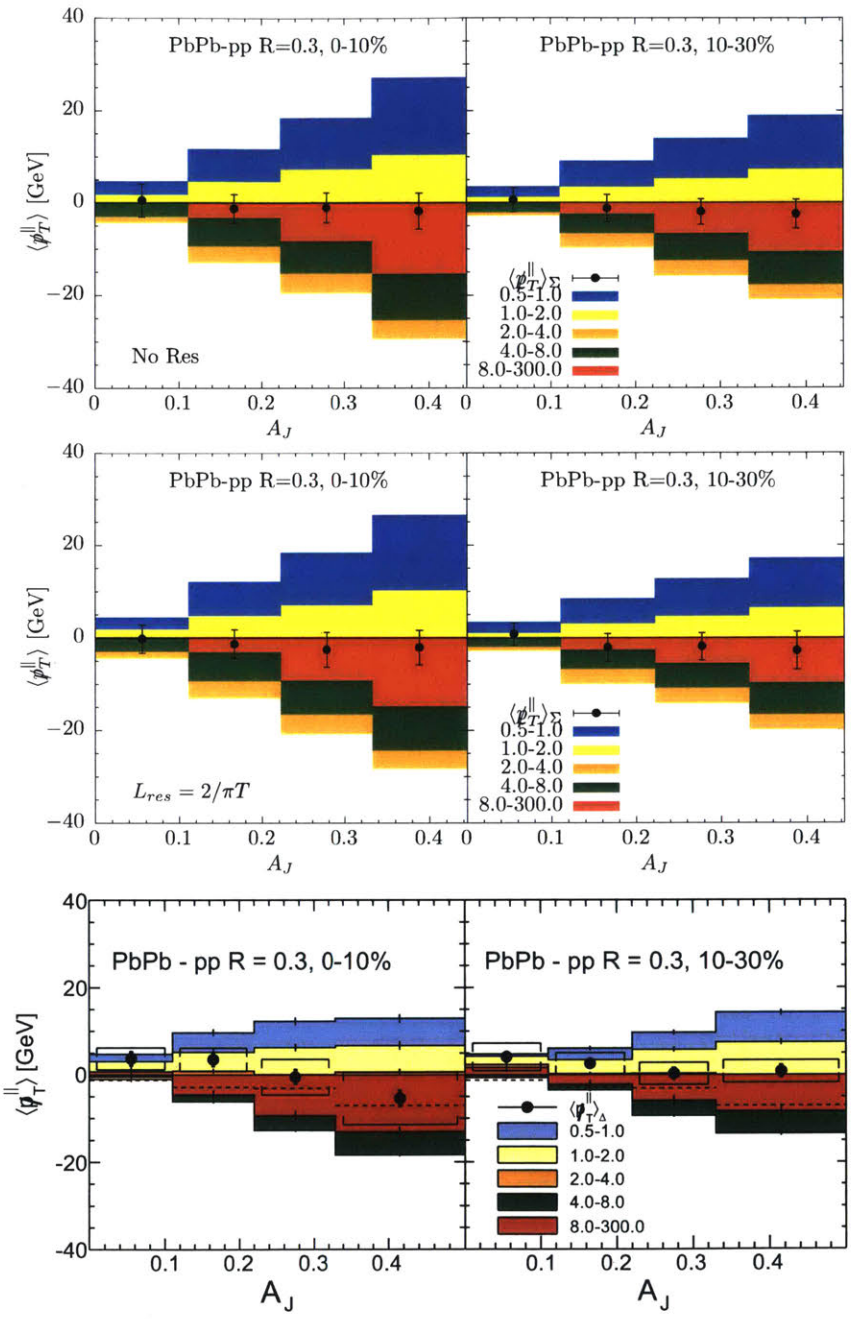

Figure 3-7: This missing P_T observable characterizes the asymmetry between the spectrum of the leading and subleading jets but this time sliced in terms of the dijet asymmetry variable, A_J. The effect of resolution can again be seen to be a slight improvement relative to data with the "orange problem" of previous works still present, albeit reduced.

Chapter 4

Discussion

In this thesis we have presented the phenomenological implications in jet quenching observables that the inability of the Quark-Gluon Plasma to resolve with arbitrary precision a collimated system of color charges has. As a first exploratory study, the characteristic resolution length of the plasma has simply been chosen to be of the order of the Debye screening length of the plasma, which is inversely proportional to the temperature, for which results both at weak and strong coupling exist. The fact that the plasma has a finite resolution length leads to the inescapable conclusion that it must perceive the propagation of a multipartonic system in terms of a collection of effective emitters. Due to the phenomenological approach to the problem, which does not incorporate the many-body quantum physics content in its whole complexity, the way in which such effective emitters are built is not free from ambiguities. We have presented what we believe to be the simplest and most consistent procedure in order to capture the essential physics of this mechanism. By exploring a reasonable set of values for the resolution distance $L_{\rm res}$, we have been able to produce results for a subset of jet and intra-jet observables by implementing the finite resolution effects within the hybrid strong/weak coupling model.

Since the number of effective energy loss sources diminishes as we increase $L_{\rm res}$, the total amount of jet energy loss decreases, so that the stopping distances, which depend on the energy and the temperature but contain a free fitting parameter $\kappa_{\rm sc}$, have to be reduced. While propagating as an effective emitter, partons lose energy in a homogeneous way, making it easier for softer particles to survive their passage through the strongly coupled

plasma. These facts can have consequences on the final intra-jet distributions as well as in the opening angle dependence of jet suppression.

First, we have seen in Fig. 3-3 how the inclusion of resolution effects mildly reduces the differences between the suppression of jets with different anti-k_t radius R, as depending on the relative separation among the different excitations between the jet, they can be perceived as a single color source from the point of view of the plasma. The absence of a clear ordering of jet R_{AA} with radius R is currently in good agreement with what is seen in data [19], although more precise measurements are needed to extract strong conclusions. More notable modifications are seen in the jet substructure of the quenched jets as reflected in the jet fragmentation functions and jet shapes. These two observables combined show how the existence of a finite resolution length helps to explain the gentle modifications experienced by the hardest and most central regions of the jet substructure, while it is shown that the dominant effect for the softest, widest structure corresponds to the contribution from the medium response.

By studying the "missing-pt" observables we have carried out a more detailed scrutiny as a function of the particle transverse momentum, and we conclude that the inclusion of the finite resolution effects is an essential piece of physics within the hybrid strong/weak coupling model which leads to a satisfactory description of the hardest momentum regions of the jet content. This fact suggests that finite resolution plays a central role in the description of high p_T hadron suppression, as the high energy region of the single particle spectrum is dominated by contributions from the jet leading tracks due to the steeply falling spectrum. We defer the study of single hadron R_{AA} and its potential sensitivity to $L_{\rm res}$ to future work.

The present study has shown that while the hybrid model with the effects of finite resolution is able to account for the modifications measured in experiments involving the hardest modes of the internal structure of single inclusive jet and dijet observables, the softer end of the spectrum crucially depends on the inclusion of the medium response due to the deposition of energy and momentum from the jet into the plasma. Although the simplified, analytical treatment of the impact on the hadronic spectra coming from the generated wake used in this work shows significant qualitative agreement with what is seen in data, it is clear that such an implementation, as already assumed by construction, fails to

describe the harder tail of the spectrum of the wake spectra. We have already outlined the successes of the Hybrid Model in characterizing the total energy loss suffered by jets as they propagate through the plasma; however, now it is clear that a full, non-approximated numerical treatment of the hydrodynamic evolution of the deposited energy with its subsequent hadronization after the freeze-out temperature is of paramount importance in order to describe those jet quenching phenomena which characterize the observables highlighted in this thesis, namely those which are sensitive to the spatial and energy distribution of the particles in the jet.

Bibliography

[1] K. Adcox et al. Formation of dense partonic matter in relativistic nucleus-nucleus collisions at RHIC: Experimental evaluation by the PHENIX collaboration. *Nucl. Phys.*, A757:184–283, 2005.

[2] I. Arsene et al. Quark gluon plasma and color glass condensate at RHIC? The Perspective from the BRAHMS experiment. *Nucl. Phys.*, A757:1–27, 2005.

[3] B. B. Back et al. The PHOBOS perspective on discoveries at RHIC. *Nucl. Phys.*, A757:28–101, 2005.

[4] John Adams et al. Experimental and theoretical challenges in the search for the quark gluon plasma: The STAR Collaboration's critical assessment of the evidence from RHIC collisions. *Nucl. Phys.*, A757:102–183, 2005.

[5] K Aamodt et al. Elliptic flow of charged particles in Pb-Pb collisions at 2.76 TeV. *Phys. Rev. Lett.*, 105:252302, 2010.

[6] Georges Aad et al. Measurement of the pseudorapidity and transverse momentum dependence of the elliptic flow of charged particles in lead-lead collisions at $\sqrt{s_{NN}} =$ 2.76 TeV with the ATLAS detector. *Phys. Lett.*, B707:330–348, 2012.

[7] Serguei Chatrchyan et al. Measurement of the elliptic anisotropy of charged particles produced in PbPb collisions at $\sqrt{s}_{NN}$=2.76 TeV. *Phys. Rev.*, C87(1):014902, 2013.

[8] Paul M. Chesler and Krishna Rajagopal. Jet quenching in strongly coupled plasma. *Phys. Rev.*, D90(2):025033, 2014.

[9] Yacine Mehtar-Tani, Carlos A. Salgado, and Konrad Tywoniuk. Anti-angular ordering of gluon radiation in QCD media. *Phys. Rev. Lett.*, 106:122002, 2011.

[10] Y. Mehtar-Tani, C. A. Salgado, and K. Tywoniuk. Jets in QCD Media: From Color Coherence to Decoherence. *Phys. Lett.*, B707:156–159, 2012.

[11] J. Casalderrey-Solana and E. Iancu. Interference effects in medium-induced gluon radiation. *JHEP*, 08:015, 2011.

[12] Jorge Casalderrey-Solana and Andrej Ficnar. Holographic Three-Jet Events in Strongly Coupled N=4 Yang-Mills Plasma. 2015.

[13] Paul M. Chesler, Kristan Jensen, Andreas Karch, and Laurence G. Yaffe. Light quark energy loss in strongly-coupled N = 4 supersymmetric Yang-Mills plasma. *Phys. Rev.*, D79:125015, 2009.

[14] Jorge Casalderrey-Solana, Doga Can Gulhan, José Guilherme Milhano, Daniel Pablos, and Krishna Rajagopal. A Hybrid Strong/Weak Coupling Approach to Jet Quenching. *JHEP*, 10:019, 2014. [Erratum: JHEP09,175(2015)].

[15] Jorge Casalderrey-Solana, Doga Can Gulhan, José Guilherme Milhano, Daniel Pablos, and Krishna Rajagopal. Predictions for Boson-Jet Observables and Fragmentation Function Ratios from a Hybrid Strong/Weak Coupling Model for Jet Quenching. *JHEP*, 03:053, 2016.

[16] Jorge Casalderrey-Solana, Doga Gulhan, Guilherme Milhano, Daniel Pablos, and Krishna Rajagopal. Angular Structure of Jet Quenching Within a Hybrid Strong/Weak Coupling Model. *JHEP*, 03:135, 2017.

[17] Dongsu Bak, Andreas Karch, and Laurence G. Yaffe. Debye screening in strongly coupled N=4 supersymmetric Yang-Mills plasma. *JHEP*, 08:049, 2007.

[18] Francesco D'Eramo, Mindaugas Lekaveckas, Hong Liu, and Krishna Rajagopal. Momentum Broadening in Weakly Coupled Quark-Gluon Plasma (with a view to finding the quasiparticles within liquid quark-gluon plasma). *JHEP*, 05:031, 2013.

[19] Vardan Khachatryan et al. Measurement of inclusive jet cross-sections in pp and PbPb collisions at $\sqrt{s_{NN}}$=2.76 TeV. *Submitted to: Phys. Rev. C*, 2016.

[20] Serguei Chatrchyan et al. Modification of jet shapes in PbPb collisions at $\sqrt{s_{NN}} = 2.76$ TeV. *Phys. Lett.*, B730:243–263, 2014.

[21] Vardan Khachatryan et al. Measurement of transverse momentum relative to dijet systems in PbPb and pp collisions at $\sqrt{s_{\mathrm{NN}}} = 2.76$ TeV. *JHEP*, 01:006, 2016.